

Torsional oscillations of a magnetar with a tangled magnetic field

Bennett Link^{*} and C. Anthony van Eysden[†]

Department of Physics, Montana State University, Bozeman, Montana, 59717, USA

5 March 2015

ABSTRACT

We propose a scenario for the quasi-periodic oscillations observed in magnetar flares wherein a tangled component of the stellar magnetic field introduces nearly isotropic stress that gives the fluid core of the star an effective shear modulus. In a simple, illustrative model of constant density, the tangled field eliminates the problematic Alfvén continuum that would exist in the stellar core for an organized field. For a tangled field energy density comparable to that inferred from the measured dipole fields of $\sim 10^{15}$ G in SGRs 1806-20 and 1900+14, torsional modes exist with fundamental frequencies of about 20 Hz, and mode spacings of ~ 10 Hz. For fixed stellar mass and radius, the model has only one free parameter, and can account for *every* observed QPO under 160 Hz to within 3 Hz for both SGRs 1806-20 and 1900+14. The combined effects of stratification and crust stresses generally decrease the frequencies of torsional oscillations by $< 10\%$ for overtones and increase the lowest-frequency fundamentals by up to 50%, and so the star can be treated as having constant density to a generally good first approximation. We address the issue of mode excitation by sudden readjustment of the stellar magnetosphere. While the total energy in excited modes is well within the energy budget of giant flares, the surface amplitude is $\lesssim 10^{-3}$ of the stellar radius for global oscillations, and decreases strongly with mode frequency. The 626 Hz QPO reported for SGR 1806-20 is particularly problematic to excite beyond a surface amplitude of 10^{-6} of the stellar radius.

Key words:

stars: neutron

1 INTRODUCTION

Soft-gamma repeaters (SGRs) are strongly-magnetized neutron stars with magnetic fields of $B = 10^{14} - 10^{15}$ G that produce frequent, short-duration bursts ($\lesssim 1$ s) of $\lesssim 10^{41}$ ergs in hard x-ray and soft gamma-rays. SGRs occasionally produce giant flares that last ~ 100 s; the first giant flare to be detected occurred in SGR 0526-66 on 5 March, 1979 (Barat et al. 1979; Mazets et al. 1979; Cline et al. 1980), releasing $\sim 2 \times 10^{45}$ erg (Fenimore et al. 1996). The August 27th 1998 giant flare from SGR 1900+14 liberated $\gtrsim 4 \times 10^{43}$ erg, with a rise time of < 4 ms (Hurley et al. 1999; Feroci et al. 1999). The duration of the initial peak was ~ 1 s (Hurley et al. 1999). On December 27, 2004, SGR 1806-20 produced the largest flare yet recorded, with a total energy yield of $\gtrsim 4 \times 10^{46}$ ergs.¹ In both short bursts and in giant flares, the peak luminosity is reached in under 10 ms. Measured spin down parameters imply surface dipole fields of 6×10^{14} G for SGR 0526-66 (Tiengo et al. 2009), 7×10^{14} G for SGR 1900+14 (Mereghetti et al. 2006), and 2×10^{15} G for SGR 1806-20 (Nakagawa et al. 2008), establishing these objects as magnetars.

^{*} E-mail: link@physics.montana.edu

[†] E-mail: anthonyvaneysden@montana.edu

¹ These energy estimates assume isotropic emission.

The giant flares in SGR 1806-20 (hereafter SGR 1806) and SGR 1900+14 (hereafter SGR 1900) showed rotationally phase-dependent, quasi-periodic oscillations (QPOs). QPOs in SGR 1806 were detected at 18 Hz, 26 Hz, 30 Hz, 93 Hz, 150 Hz, 626 Hz, and 1837 Hz (Israel et al. 2005; Watts & Strohmayer 2006; Strohmayer & Watts 2006; Hambaryan et al. 2011). QPOs in the giant flare of SGR 1900 were detected at 28 Hz, 53 Hz, 84 Hz, and 155 Hz (Strohmayer & Watts 2005). Recently, oscillations at 57 Hz were identified in the short bursts of SGR 1806 (Huppenkothen et al. 2014), and at 93 Hz, 127 Hz, and possibly 260 Hz in SGR J1550-5418 (Huppenkothen et al. 2014).² Overall, the data show that SGRs 1806 and 1900 support oscillations with spectra that begin at about 20 Hz, with a spacing of some tens of Hz below 160 Hz. The relative dearth of high-frequency QPOs could indicate a sparse spectrum above 160 Hz, or highly-preferential mode excitation. Given that we do not understand how surface oscillations affect magnetospheric emission, it could be that some modes are not seen because they do not create large changes in the x-ray emissivity for our viewing angle.

Duncan (1998) predicted that the most energetic magnetar flares would excite observable seismic modes of the neutron star crust. The easiest modes to excite, Duncan argued, would be torsional oscillations which, for the assumed composition, begin at about 30 Hz. The fundamental torsional mode consists of periodic twisting of two hemispheres in opposite directions. Crust rigidity provides the restoring force, and the star oscillates as a torsion pendulum.

Initial theoretical study of the observed QPOs treated the crust and core as uncoupled for simplicity (Piro 2005; Samuelsson & Andersson 2007; Lee 2007; Sotani et al. 2007; Watts & Reddy 2007; Sotani et al. 2007; Steiner & Watts 2009). As pointed out by Levin (2006), however, the strong magnetic field of a magnetar introduces an essential complication; the charged component of the fluid core, primarily protons and electrons, supports Alfvén waves that couple to the highly-conductive crust and affect the mode spectrum. A neutron star therefore cannot be regarded as possessing crust modes that are separate from the core, rather, we must consider *global* oscillations of the crust-core system (Levin 2006; Glampedakis et al. 2006).

It has become clear that the nature of the Alfvén wave spectrum of the core plays a crucial role in the global magneto-elastic problem. For smooth magnetic field geometries, such as uniform magnetization or a dipole field, the core fluid can be regarded as supporting an *Alfvén continuum* of frequencies; each frequency corresponds to a natural frequency of a magnetic field line. Since there is a continuous distribution of line lengths through some range, the spectrum is continuous. Dipolar field geometries and their extensions generally give a core spectrum with continuous *bands* separated by *gaps*, and a low-frequency cut-off or *edge*, much like electronic band structure in solids. The crust, by contrast, supports only a discrete spectrum of torsional modes if isolated from the core. When the crust is included and coupled to the core fluid through magnetic stresses, the structure of the core spectrum leads to very rich dynamics as shown by Levin (2007) for a simple model with a thin crust and a core of constant magnetization. If energy is deposited in the crust at one of the natural frequencies of the crust, and this frequency lies within a portion of the core continuum, the energy is lost to the core continuum in less than 0.1 s as the entire core continuum is excited. The crust excitation is effectively damped through *resonant absorption*, a familiar process in MHD; see *e.g.*, Goedbloed & Poedts (2004).

The turning points and edges in the Alfvén continuum play a special role in the dynamics; power rests at these points and gives QPOs. Subsequent work on purely fluid stars in general-relativistic MHD with more realistic field geometries also showed oscillations near the continuum edges (Sotani et al. 2007, 2008; Cerdá-Durán et al. 2009; Colaiuda et al. 2009; Cerdá-Durán et al. 2009). van Hoven & Levin (2011) have shown that if a natural frequency of the free crust happens to fall within a gap, there is little loss of the crust’s oscillation energy to the core by resonant absorption; see also work by Colaiuda & Kokkotas (2011). Frequency drift, due to the effects of the continuum, generally occurs (van Hoven & Levin 2011). This basic picture has been further developed and refined (Gabler et al. 2011; Colaiuda & Kokkotas 2011; Gabler et al. 2012; van Hoven & Levin 2012; Passamonti & Lander 2013; Gabler et al. 2013a,b, 2014). In particular, Colaiuda & Kokkotas (2011) find that all observed QPOs in SGRs 1806 and 1900 can be accommodated with a particular arrangement of continuum gaps. Colaiuda & Kokkotas (2012) find in a spherical model with a magnetic field with both poloidal and toroidal components that peaks below about 100 Hz can persist in the power spectrum, though these peaks are far broader than observed. Gabler et al. (2013a), Gabler et al. (2013b), Passamonti & Lander (2013), and Passamonti & Lander (2014) find a small number of low-frequency QPOs that exist in the continuum gaps and at turning points for their assumed field geometries that agree qualitatively with observations. Superfluidity widens the gaps in the Alfvén continuum (Gabler et al. 2013b; Passamonti & Lander 2014).

Most of the work on the global oscillation problem described above relies on tuning the locations of the gaps and turning points in the Alfvén continuum to accommodate the observed QPOs. Here we take a rather different view than in previous work, and assert that the Alfvén continuum that has been so problematic is unlikely to exist at all. The Alfvén continuum results from assuming *smooth*, poloidal field configurations. Given the convective dynamo that is expected to operate in a proto-magnetar, and subsequent evolution of the initial field, we expect the field to have high-order evolving multipoles. We conjecture that the field is complex and tangled over length scales small compared to the stellar radius, and smooth only on average. High-order multipoles (the tangle), could be long lived in the core where the electrical conductivity is high. van

² El-Mezeini & Ibrahim (2010) reported evidence for oscillations in the short, recurring bursts of SGR 1806, but this analysis was shown by Huppenkothen et al. (2013) to be flawed.

Hoven & Levin (2011) have argued that a highly-tangled field is likely to reduce or eliminate the importance of the Alfvén continuum and to give an effective shear modulus to the core fluid; they demonstrated that the continuum is broken for a “box” neutron star.

Much work on the QPO problem has included realistic neutron structure, specific magnetic field geometries, and the effects of general relativity. Given that the interior field geometry will likely remain unknown, we take a step back in sophistication and propose a minimal, illustrative model of the low-frequency magnetar QPOs (< 160 Hz). The star is essentially a self-gravitating, constant-density, magnetized fluid whose oscillation frequencies are determined by the anisotropic magnetic stresses from the large-scale organized field (primarily the dipole component) and the approximately isotropic magnetic stresses introduced by the tangled field; we show that density stratification and the crust typically change the oscillation frequencies by only $\sim 10\%$ (though 30-50% for some fundamental modes), so this simple model is an adequate first approximation for developing a quantitative understanding of torsional modes, while elucidating the essential physics. General relativity is included only as a redshift factor that reduces the oscillation frequencies observed at infinity by about 20%. We show that if the energy density in the tangled field is comparable to that in the large-scale field, a discrete normal mode spectrum beginning at around 20 Hz with a spacing of 10 Hz appears naturally for axial modes, generally consistent with observations of QPOs below 160 Hz, and that all QPOs observed in SGRs 1806 and 1900 in this frequency range can be accounted for to within 3 Hz. We do not address the character of high-frequency modes due to limitations to our model that we describe. To illustrate the key features of the model, the normal-mode analysis will be restricted entirely to axial modes. (We use the terms “axial” and “torsional” synonymously).

In §2 we derive the equations of motion for a star with a tangled field, and show how the tangled field gives the core fluid an effective shear modulus. In §3, we briefly review how an Alfvén continuum arises for a uniform field. In §4, we present analytic solutions for a star with only a tangled field; these solutions are useful for understanding the results of a more general field configuration consisting of an organized field plus a tangled field, described in §5. In §6, we show that realistic stellar structure and crust stresses both have relatively small effects on most of the eigenfrequencies for torsional modes if the energy density in the tangled field is comparable to or larger than that in the organized field. In §7, we study the energetics of QPO excitation. In §8, we discuss the implications of our work, our key results, limitations of the model, and future improvements. In Appendix A, we describe the variable separation procedure we used to obtain the solutions of §5. In Appendix B, we use a simple model to show why the crust has a negligible effect.

2 EQUATIONS OF MOTION

The matter is subject to magnetic and material stresses. We will find that QPOs in SGRs 1806 and 1900 can be explained by average magnetic fields above 10^{15} G, comparable to the upper critical field for superconductivity, so we take the star to be a normal conductor. The dipole field could be much smaller than the average field, and will not affect the basic picture provided the protons are normal; we do not consider the effects of superconducting protons in this preliminary study.

The stress tensor for matter permeated by a field \mathbf{B} is

$$T_{ij} = \frac{1}{4\pi} \left[B_i B_j - \frac{1}{2} B^2 \delta_{ij} \right] + \mu (\nabla_i u_j + \nabla_j u_i). \quad (1)$$

where μ is the shear modulus of the crust. We assume a perfect conductor, so that perturbations in the field satisfy

$$\delta \mathbf{B} = \nabla \times (\mathbf{u} \times \mathbf{B}), \quad (2)$$

where \mathbf{u} is the displacement vector of a mass element. We specialize to shear perturbations, so that $\nabla \cdot \mathbf{u} = 0$, for which eq. (2) becomes

$$\delta \mathbf{B} = (\mathbf{B} \cdot \nabla) \mathbf{u} - (\mathbf{u} \cdot \nabla) \mathbf{B}. \quad (3)$$

For a displacement \mathbf{u} , the stress tensor is perturbed by

$$\delta T_{ij} = \frac{1}{4\pi} \left[B_j B_k \nabla_k u_i - B_j u_k \nabla_k B_i - \frac{1}{2} \delta_{ij} B_k B_l \nabla_l u_k + \frac{1}{2} \delta_{ij} B_k u_l \nabla_l B_k \right] + \mu \nabla_i u_j + \text{transpose}, \quad (4)$$

where repeated indices are summed and μ is the shear modulus of the matter, non-zero only in the crust, and B_i denotes a component of the unperturbed field. We include μ here only for completeness; we will ultimately find that material stresses are dominated by those from the tangled field.

We treat the magnetic field as consisting of an organized, largely dipolar contribution \mathbf{B}_o , plus a much more complicated tangled component \mathbf{B}_t :

$$\mathbf{B} = \mathbf{B}_o + \mathbf{B}_t. \quad (5)$$

We assume that the field is tangled for length scales smaller than l_t , small compared to the stellar radius. Given the uncertainties in the overall field structure, we take \mathbf{B}_o constant for simplicity. We denote volume averages over l_t^3 as $\langle \dots \rangle$. We

assume that different components of the tangled field are uncorrelated on average. Under this assumption, the tangled field can contribute only isotropic stress over length scales above l_t , so that

$$\langle B_i B_j \rangle = B_i^o B_j^o + \langle B_t^2 \rangle \delta_{ij}, \quad (6)$$

where $\langle B_t^2 \rangle$ is a constant.

To treat the tangled field's contribution to the stress, we average the perturbed stress tensor of eq. (4). Eqs. (4) and (6) to obtain

$$\langle \delta T_{ij} \rangle = \frac{1}{4\pi} \left[\langle B_j B_k \rangle \nabla_k u_i - u_k \langle B_j \nabla_k B_i \rangle - \frac{1}{2} \delta_{ij} \langle B_k B_l \rangle \nabla_l u_k + \frac{1}{2} \delta_{ij} u_l \langle B_k \nabla_l B_k \rangle \right] + \mu \nabla_i u_j + \text{transpose}, \quad (7)$$

where u_i now denotes a component of the displacement field averaged over l_t^3 .

If different components of the tangled field are uncorrelated over l_t^3 , one component will also be uncorrelated with the gradient of a different component, that is,

$$\langle B_i \nabla_k B_j \rangle = \langle (B_i^o + B_i^t) \nabla_k (B_j^o + B_j^t) \rangle = \langle B_i^t \nabla_k B_j^t \rangle = 0 \quad i \neq j. \quad (8)$$

Since the tangled field varies over length scales smaller than l_t , a component of the tangled field will also be uncorrelated with the gradient of the same component, so that

$$\langle B_i^t \nabla_k B_i^t \rangle = 0, \quad (9)$$

which applies component by component, and therefore also in summation, as given above. Using eqs. (6), (8), (9), and $\nabla \cdot \mathbf{u} = 0$, eq. (7) becomes

$$\langle \delta T_{ij} \rangle = \frac{1}{4\pi} \left(B_j^o B_k^o \nabla_k u_i + B_i^o B_k^o \nabla_k u_j - \delta_{ij} B_k^o B_l^o \nabla_l u_k \right) + \left(\frac{1}{4\pi} \langle B_t^2 \rangle + \mu \right) (\nabla_i u_j + \nabla_j u_i). \quad (10)$$

The tangled field gives the fluid an effective shear modulus of $\langle B_t^2 \rangle / 4\pi$, and enhances the rigidity of the solid.

Upon comparing our mode calculations with data, we will find that the total energy in shear waves in the core greatly dominates that in the crust. We henceforth ignore crust rigidity, and justify this approximation in §5 and Appendix B.

We will be interested in modes with wavelengths greater than l_t , for which the equation of motion is

$$\rho_d \frac{\partial^2 u_j}{\partial t^2} = \nabla_i \langle \delta T_{ij} \rangle, \quad (11)$$

where ρ_d is the dynamical mass density of matter that is frozen to the magnetic field. If the protons are normal, as we have assumed, there will no entrainment between the protons and neutrons; entrainment of the neutrons is in any case a small effect if the both the protons and neutrons are superfluid (Chamel & Haensel 2006). We take ρ_d to be the proton density $x_p \rho$, where ρ is the mass density, and $x_p \sim 0.1$ is the average proton mass fraction in the core.

We neglect coupling of the stellar surface to the magnetosphere, and treat the surface as a free boundary with zero traction, thus ignoring momentum flow into the magnetosphere. Under this assumption, the traction at the surface vanishes:

$$\hat{r}_i \langle \delta T_{ij} \rangle = 0, \quad (12)$$

where \hat{r} is the unit vector normal to the stellar surface.

Given the uncertainties in the field geometry, we henceforth consider a uniform star of density $\rho = 3M/4\pi R^3$ for illustration, where M and R are the stellar mass and radius, and take $\mathbf{B}_o = \hat{z} B_o$ where B_o is constant. Eqs. (10) and (11) give

$$c_o^2 \frac{d^2 \mathbf{u}}{dz^2} - c_o^2 \nabla \frac{du_z}{dz} + c_t^2 \nabla^2 \mathbf{u} + \omega^2 \mathbf{u} = 0, \quad (13)$$

where $c_o^2 \equiv B_o^2 / (4\pi \rho_d)$ and $c_t^2 \equiv \langle B_t^2 \rangle / (4\pi \rho_d)$; c_o is the speed of Alfvén waves supported by the organized field, and c_t is the speed of transverse waves supported by the isotropic stress of the tangled field. We show in §6 that realistic stellar structure changes the eigenfrequencies of torsional modes by typically $\sim 10\%$ (but by up to $\sim 50\%$ for the lowest-frequency fundamentals), so that a constant-density model is a good first approximation.

3 THE ALFVÉN CONTINUUM

For finite \mathbf{B}_o and $\mathbf{B}_t = 0$, there exists a continuum of axial modes (Levin 2007), given by eq. (13)

$$c_o^2 \frac{d^2 \mathbf{u}}{dz^2} - c_o^2 \nabla \frac{du_z}{dz} + \omega^2 \mathbf{u} = 0, \quad (14)$$

In cylindrical coordinates (s, ϕ, z) , axial modes are given by $\mathbf{u} = u_\phi \hat{\phi}$. For a constant field, and no crust, field lines have a continuous range of lengths between zero and $2R$, determined by the cylindrical radius s . Within the approximation of

ideal MHD, fluid elements at different cylindrical radii cannot exchange momentum. At a given s , the length of a field line is $2\sqrt{R^2 - s^2}$. The solutions have even parity ($\cos kz$) and odd parity ($\sin kz$). The requirement that the traction vanish at the stellar surface gives the spectrum

$$\nu_n = \frac{n}{2} \frac{c_o}{\sqrt{R^2 - s^2}} \quad \text{even parity} \quad (15)$$

$$\nu_n = \frac{(2n+1)}{4} \frac{c_o}{\sqrt{R^2 - s^2}} \quad \text{odd parity.} \quad (16)$$

where n is an integer, beginning at zero for the odd-parity modes, and $\nu = \omega/2\pi$. Because s is a continuous variable, for every n there is a continuous spectrum of modes for this simple magnetic geometry. An infinite sequence of continua begins at $\sim 7(2n+1) B_{15}^o$ Hz for odd-parity modes and $\sim 7(2n) B_{15}^o$ Hz for the even-parity modes, where $B_{15}^o \equiv B_o/(10^{15} \text{ G})$. The full spectrum begins at $\sim 7 B_{15}^o$ Hz; there is also a zero-frequency mode corresponding to rigid-body rotation. The same conclusion holds for more general axisymmetric field geometries, though certain geometries give gaps in the continuum.

4 ISOTROPIC MODEL

We now turn to the opposite extreme of a tangled field that dominates the stresses, taking $\mathbf{B}_o = 0$, and solving the resulting isotropic problem. This problem provides useful insight into the mode structure of the more general problem with non-zero \mathbf{B}_o and $\langle B_t^2 \rangle$. For this case, eq. (13) becomes

$$c_t^2 \nabla^2 \mathbf{u} + \omega^2 \mathbf{u} = 0, \quad (17)$$

Subject to the restriction $\nabla \cdot \mathbf{u} = 0$, the solutions for spheroidal modes ($u_r = 0$), can be separated as

$$u_\phi = w(r) \frac{\partial}{\partial \theta} Y_{lm}(\theta, \phi) e^{i\omega t} \quad (18)$$

$$u_\theta = -w(r) \frac{1}{\sin \theta} \frac{\partial}{\partial \phi} Y_{lm}(\theta, \phi) e^{i\omega t}. \quad (19)$$

The radial function $w(r)$ satisfies Bessel's equation:

$$\left(\frac{d^2}{dr^2} + \frac{2}{r} \frac{d}{dr} - \frac{l(l+1)}{r^2} + k^2 \right) w(r) = 0, \quad (20)$$

where $k \equiv \omega/c_t$.

The solutions that are bounded at $r = 0$ are the spherical Bessel functions $j_l(kr)$. Zero traction at the stellar surface gives

$$\left[\frac{dj_l}{dr} - \frac{j_l}{r} \right]_{r=R} = 0 \quad (21)$$

For each value of l , eq. (21) has solutions $x_{l,n} \equiv k_{l,n} R$, where $n = 0, 1, 2, \dots$, the overtone number, gives the number of nodes in $j_l(r)$. The eigenfrequencies are

$$\omega_{l,n} = \left(1 - \frac{R_s(M)}{R} \right)^{1/2} \left(\frac{\langle B_t^2 \rangle R}{3x_p M} \right)^{1/2} x_{l,n} \quad (22)$$

where a redshift factor $z \equiv (1 - R_s(M)/R)^{1/2}$ has been introduced; R_s is the Schwarzschild radius. In terms of fiducial values

$$\nu_{l,n}(\text{Hz}) = \frac{\omega_{l,n}}{2\pi} = 4.3 \left(\frac{z}{0.77} \right) \left(\frac{R}{10 \text{ km}} \right)^{1/2} \left(\frac{M}{1.4 M_\odot} \right)^{-1/2} \left(\frac{x_p}{0.1} \right)^{-1/2} \left(\frac{\langle B_t^2 \rangle^{1/2}}{10^{15} \text{ G}} \right) x_{l,n} \text{ Hz.} \quad (23)$$

In Table 1, we give some of the eigenfrequencies for these fiducial values. We note that for $\langle B_t^2 \rangle^{1/2} = 10^{15} \text{ G}$, this simple model gives fundamental frequencies below 20 Hz, with a spacing of about 15 Hz for the overtones.

For $l = 1$, eq. (21) has a solution $w(r) = r$ for $k = 0$. This solution corresponds to rigid-body rotation and we label it $n = 0$. This solution is of no physical significance to the mode problem we are addressing, but we include it in Tables 1-3 for completeness.

Frequencies above 160 Hz correspond to $k_{n,l} R \gtrsim 30$, or wavelengths $\lesssim 0.2R$. At these high wavenumbers, the wavelength of the mode could be comparable to or smaller than the length scale l_t over which the field can be considered tangled, in which case the averaging procedure of §2 would break down. In this case, the mode frequencies will be determined, at least in part, by the detailed (and unknown) field geometry. Henceforth, we restrict the analysis to $\nu < 160 \text{ Hz}$, the range in which the low-frequency QPOs lie.

l	$n = 0$	$n = 1$	$n = 2$	$n = 3$	$n = 4$	$n = 5$	$n = 6$
1	0	24	39	52	66	79	93
2	11	30	45	58	72	85	99
3	16	36	50	64	78	92	105
4	22	41	56	70	84	98	111
5	27	46	61	76	90	103	117
6	31	52	67	81	95	109	123

Table 1. Eigenfrequencies in Hz for the fiducial values of eq. (23).

5 ANISOTROPIC MODEL

We now turn to the general problem of non-zero \mathbf{B}_o and $\langle B_t^2 \rangle$, and show that even a small amount of stress from the tangled field breaks the Alfvén continuum very effectively. The normal modes of the system are similar to those found in the isotropic problem for $\langle B_t^2 \rangle \simeq B_o^2$.

The modes are given by eq. (13). This vector equation, subject to boundary conditions on the surface of a sphere, is difficult to solve in general. For illustration, we specialize to axial modes, $u_\theta = u_r = 0$, giving in cylindrical coordinates (s, ϕ, z) :

$$c_o^2 \frac{d^2 u_\phi}{dz^2} + c_t^2 \nabla^2 u_\phi - c_t^2 \frac{u_\phi}{s^2} + \omega^2 u_\phi = 0. \quad (24)$$

The third term results from derivatives of $\hat{\phi}$ in the original vector equation (13). Defining $b_t^2 \equiv \langle B_t^2 \rangle / B_o^2$, the ratio of the energy density in the tangled field to that in the organized field, the above equation becomes

$$c_o^2 \left[b_t^2 \frac{1}{s} \frac{\partial}{\partial s} \left(s \frac{\partial u_\phi}{\partial s} \right) + (1 + b_t^2) \frac{\partial^2 u_\phi}{\partial z^2} - b_t^2 \frac{u_\phi}{s^2} \right] + \omega^2 u_\phi = 0. \quad (25)$$

The zero-traction boundary condition (eq. 12) at the stellar surface is

$$b_t^2 \left(s \frac{\partial u_\phi}{\partial s} - u_\phi \right) + (1 + b_t^2) z \frac{\partial u_\phi}{\partial z} = 0. \quad (26)$$

Equation (25) is solved in the domain $z \geq 0$, and so at $z = 0$ we require

$$u_\phi = 0, \quad (27)$$

for modes with *odd* parity about $z = 0$, and

$$\frac{\partial u_\phi}{\partial z} = 0, \quad (28)$$

for modes with *even* parity. The system is separable with a coordinate transformation; the details are given in Appendix A. We solve eqs. (A8), (A9), and (A10) numerically to obtain the normal mode frequencies. The solutions are given by two quantum numbers: κ and the overtone number n . κ maps smoothly to $l(l+1)$ in the limit $c_o^2 \rightarrow 0$, so we use l and n for convenience in labeling the modes. We refer to $n = 0$ for a given l as the fundamental for that value of l .

The mode structure is shown in Figure 1 for constant *total* magnetic energy, with $(B_o^2 + \langle B_t^2 \rangle)^{1/2}$ fixed at 10^{15} G. Modes for which u_ϕ has even parity (odd l) and odd parity (even l) about $z = 0$ have been plotted separately. For large b_t^2 the isotropic solution presented in Table 1 is recovered. As b_t^2 is reduced, the modes become more closely spaced, approaching a continuum as $b_t^2 \rightarrow 0$. In the limit $b_t^2 \rightarrow 0$ the sequence of continua begins at $\sim 7(2n+1)$ Hz for odd-parity modes (even l) and $\sim 14n$ Hz for even-parity modes (odd l), in agreement with the continuum sequences described by eqs. (15) and (16). The $n = 0$ odd modes approach zero as $b_t^2 \rightarrow 0$ and scale as

$$\nu = 6.70 l b_t \left(\frac{z}{0.77} \right) \left(\frac{R}{10 \text{ km}} \right)^{1/2} \left(\frac{M}{1.4 M_\odot} \right)^{-1/2} \left(\frac{x_p}{0.1} \right)^{-1/2} \left(\frac{B_o}{10^{15} \text{ G}} \right) \text{ Hz}. \quad (29)$$

These modes approach rigid-body rotation solutions of the continuum coupled together by the tangled field in the $b_t \rightarrow 0$ limit. Examination of the eigenmodes as $b_t^2 \rightarrow 0$ also shows that the oscillation amplitude becomes sharply peaked at a specific value of the cylindrical radius s and vanishes everywhere else, in agreement with the continuum solution in §3.

The splitting of the Alfvén continuum is shown in a different way in Figure 2, where realistic predictions are made for the eigenfrequencies in SGR 1806 (left) and 1900 (right). In contrast with Figure 1 where the *total* magnetic field was held constant ($(B_o^2 + \langle B_t^2 \rangle)^{1/2} = 10^{15}$ G), we now fix the *ordered* field B_o in each magnetar to its observed dipole spin-down value: 7×10^{14} G for SGR 1806 and 2×10^{15} G for SGR 1900. We take the fiducial values of $M = 1.4 M_\odot$, $R = 10$ in each magnetar. Eigenfrequencies for all n and l for the range of frequencies shown are plotted. For $b_t^2 = 0$, there exists an Alfvén continuum that begins at $\simeq 7 B_{15}^\circ$ Hz, with a zero-frequency solution corresponding to rigid-body rotation. As b_t^2 is

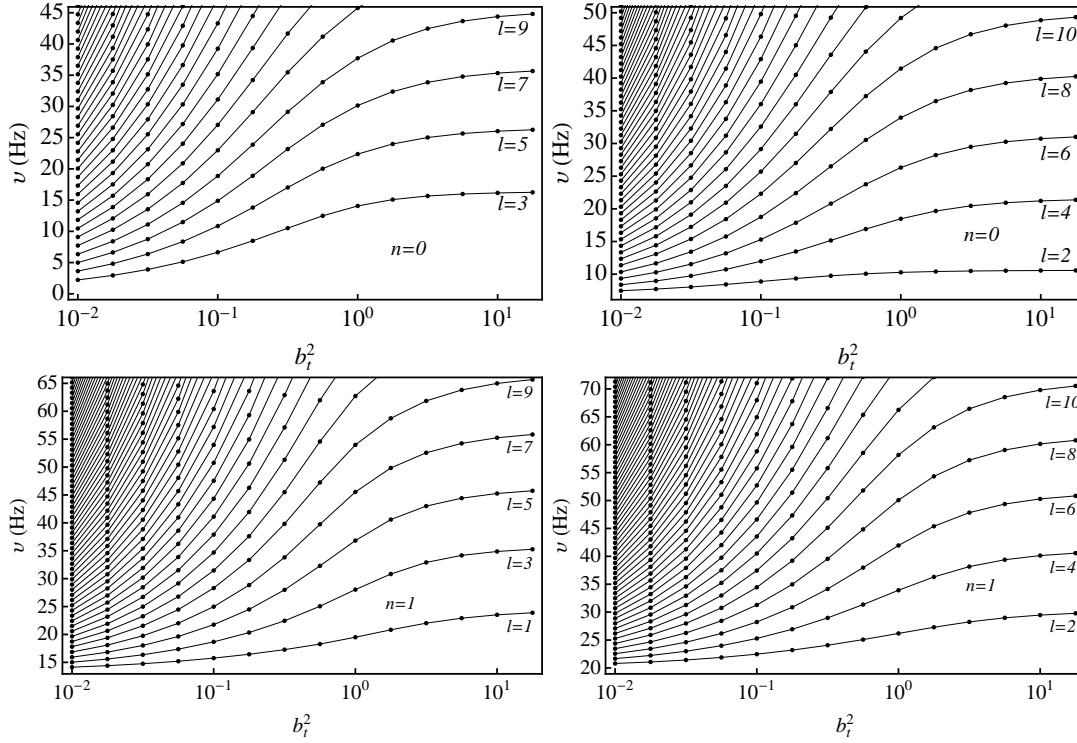


Figure 1. Splitting of the Alfvén continuum as a tangled field is added to a smooth field. We have fixed $(B_0^2 + \langle B_t^2 \rangle)^{1/2} = B_0(1 + b_t^2)^{1/2}$ to 10^{15} G to illustrate the smooth transition from the continuum to the isotropic tangle. For l odd and $n = 0$ (upper left panel), low-frequency modes exist that go to zero frequency for $b_t^2 \rightarrow 0$; see equation (29).

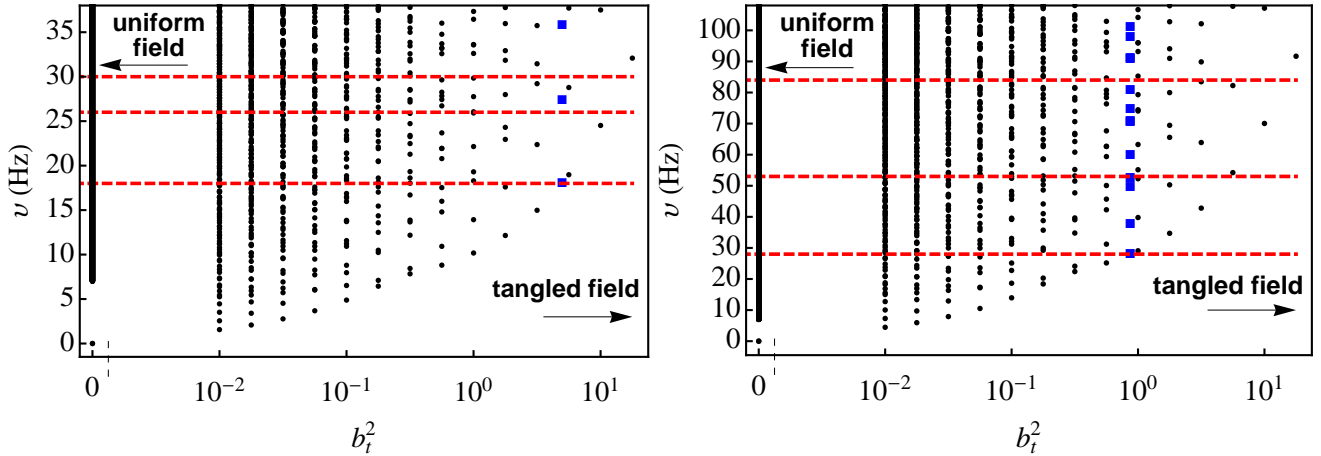


Figure 2. Splitting of the Alfvén continuum (the column on the far left of each figure) as a tangled field is added to a smooth field in SGR 1806 (left) and 1900 (right). The ordered field is fixed at the dipole spin-down value: 2×10^{14} for SGR 1806 and 2×10^{15} for SGR 1900. Red-dashed lines correspond to observed QPO frequencies. Solid-blue squares represent the value of b_t^2 that best fits the data in each object, though note that only three observed QPOs are shown on the scales of these plots. The lowest sequence of points approach the $k = 0$ rigid-body mode (not shown here), according to eq. (29).

increased, the continuum splits into discrete normal modes. As b_t^2 is further increased and the modes spread out further, the higher-frequency modes move off the diagram. For large b_t^2 the eigenfrequencies become large due to the large tangled field.

The observed QPO frequencies in SGRs 1806 and 1900 are shown in Figure 2 as horizontal red dashed lines. For given M and R , the model has only b_t^2 as a free parameter, and gives quantitative predictions. Assuming the lowest observed QPO corresponds to the lowest eigenfrequency in the spectrum fixes the value of b_t^2 in each object, giving 5.0 and 0.87 for SGR 1806s and 1900 respectively. Eigenfrequencies for these b_t^2 are plotted as solid blue squares.

In Tables 2 and 3, we give frequencies for SGR 1806 and 1900 at $b_t^2 = 5.0$ and 0.87 respectively. Numbers in boldface denote normal mode frequencies that are within 3 Hz of an observed QPO in both SGRs 1806 and 1900, and represent

l	$n = 0$	$n = 1$	$n = 2$	$n = 3$	$n = 4$	$n = 5$	$n = 6$
1	0	39	62	85	108	130	153
2	18	49	73	96	119	142	
3	27	58	81	104	126	148	
4	36	67	91	114	137	160	
5	44	76	100	123	145		
6	52	84	109	133	155		
7	59	93	118	142			

Table 2. Eigenfrequencies in Hz for SGR 1806 with $B_o = 7 \times 10^{14}$ and $b_t^2 = 5.0$. Numbers in boldface are within 3 Hz of an observed QPO, and represent plausible mode identifications. We do not list frequencies above 160 Hz.

l	$n = 0$	$n = 1$	$n = 2$	$n = 3$
1	0	52	89	126
2	28	71	108	144
3	38	75	109	145
4	50	91	127	
5	60	98	130	
6	70	112	147	
7	81	121	152	
8	91	134		
9	101	144		
10	111	155		

Table 3. Eigenfrequencies in Hz for SGR 1900 with $B_o = 2 \times 10^{15}$ and $b_t^2 = 0.87$. Numbers in boldface are within 3 Hz of an observed QPO, and represent plausible mode identifications. We do not list frequencies above 160 Hz.

plausible mode identifications. Within these tolerances, *every observed QPO frequency below 160 Hz in SGRs 1806 and 1900 is accounted for*. For SGR 1806, the model does not give the distinct 26 Hz and 30 Hz that have been reported, but we note that these features are quite broad (Watts & Strohmayer 2006). The reported frequencies have uncertainties, and drift with time, and analysis has not yet been done to determine if the data favor two frequencies around 26-30 Hz, or only one. In our model, both are accommodated by the 27 Hz frequency for this example. If distinct QPOs at 26 and 30 Hz could be ascertained, this would challenge our model.

Examples of eigenmodes are plotted in Figure 3. The left panel shows the 93 Hz mode of SGR 1806, with the attribution $l = 7, n = 1$, while the right panel shows the 155 Hz of SGR 1806, with the attribution $l = 10, n = 1$. The left panel has $b_t^2 = 5.0$, which is close to the isotropic limit, and shows a large degree of spherical structure symmetry. In the plot on the right, $b_t^2 = 0.87$, and the mode shows mostly cylindrical structure, a characteristic feature of the continuum.

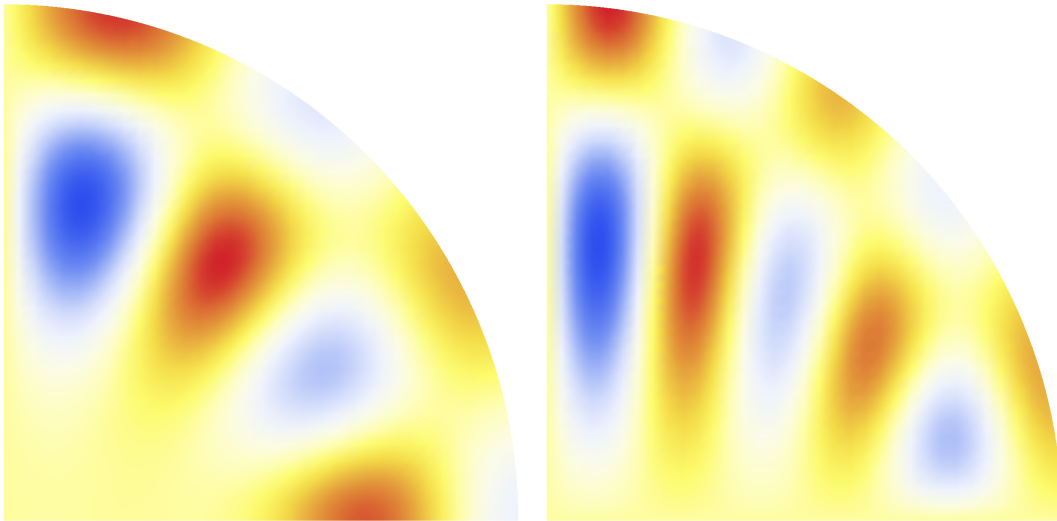


Figure 3. Example eigenmodes for SGR 1806s (left) and 1900 (see text for details). Blue denotes motion out of the page for a given phase, red denotes into the page, and white denotes zero amplitude. The left panel has $b_t^2 = 5$ and exhibits the spherical structure of the isotropic limit, while the right has $b_t^2 = 0.86$ and exhibits the cylindrical structure of the continuum.

l	$n = 0$	$n = 1$	$n = 2$	$n = 3$	$n = 4$	$n = 5$	$n = 6$
1	0	-15%	-15%	-16%	-15%	-16%	-16%
2	+48%	-8.9%	-12%	-14%	-15%	-15%	-15%
3	+41%	-4.5%	-10%	-12%	-13%	-14%	-14%
4	+35%	-1.9%	-8.0%	-11%	-12%	-13%	-14%
5	+31%	-0.47%	-6.5%	-9.4%	-11%	-12%	-13%
6	+27%	0.33 %	-5.6%	-8.5%	-10%	-11%	-12%

Table 4. Percentage frequency change of modes in a stratified star with a crust compared with a constant density star with the same mass and radius. We use a $1.4 M_{\odot}$ star with radius 13.1 km, taking $x_p = 0.1$, and magnetic field $\langle B_t^2 \rangle = 10^{15}$ G

Though our simple, constant density model is intended mostly for illustration, it accurately reproduces all observed QPOs in SGRs 1806 and 1900 though the spectrum is rather dense with a spacing of about 10 Hz. The main goal has been to show in a quantitative manner how the Alfvén continuum is broken. As we show in §6, the effects of realistic stellar structure are generally small (except for low- l fundamentals), and so this constant-density model is sufficiently accurate for semi-quantitative study of torsional oscillations. Many of the predicted frequencies have not been observed, and we discuss this further below.

All examples shown here are for $R = 10$ km. If R is reduced, it is necessary to decrease b_t^2 to obtain similar fits to the data. The spectrum becomes generally less dense. Larger R has the opposite effect.

6 EFFECTS OF STRATIFICATION AND THE CRUST

We now show that density stratification and crust rigidity gives corrections to the eigenfrequencies of the constant-density model considered thus far of typically $\sim 10\%$, but up to 50% for low- l fundamentals. Because our best fits to the data for the constant-density model give $b_t^2 = 5$ for SGR 1806 and $b_t^2 \sim 1$ for SGR 1900, we ignore the organized field, and study the isotropic problem corresponding to a strong magnetic tangle.

We construct a relativistic star using the analytic representation of the Brussels-Montreal equation of state derived by Potekhin et al. (2013). For a $1.4 M_{\odot}$ neutron star, we obtain a radius of 13.1 km. We take $x_p = 0.1$, and fix the magnetic field at $\langle B_t^2 \rangle = 10^{15}$ G. The shear modulus is from Strohmayer et al. (1991). For this spherical problem, the variable separation proceeds as in §4. We solve numerically for the radial eigenfunctions and eigenfrequencies. As a baseline for comparison, Table 1 can be scaled according to eq. (23) to obtain the eigenfrequencies for a constant-density star of radius 13.1 km. We assume that the dynamical density in the crust is equal to the total mass density, so that the entrainment of superfluid neutrons in the crust Chamel (2005, 2012) is effectively perfect. Entrainment, or lack of entrainment, has little effect on our results.

To explore the individual effects of stratification and the crust, we first examined a stratified star with no crust. We find that stratification lowers the frequencies for all modes with the exception of the $n = 0$ modes, which are raised; typical changes are $< 20\%$ for $n = 0$ and -15% for $n > 0$. This general trend was also found by Passamonti & Lander (2014). The reason for the frequency decrease (except for $n = 0$) can be seen by noting that the frequency scales as $R^{1/2}$ in the case of uniform density; see eq. (23). The stratified star has more mass concentrated in the central regions of the star, making it behave effectively as a smaller star compared to a constant-density star of the same radius.

Next, we considered a stratified star with a crust. The addition of a crust increases all frequencies by $\sim 5 - 20\%$ for $n = 0$ and $1-5\%$ for $n > 0$ compared with the stratified case. The crust increases the frequency because it increases the average shear modulus of the star. The effect is small because the shear modulus of the crust exceeds $\langle B_t^2 \rangle / 4\pi$ in only a small fraction of the stellar volume. The effects of crust rigidity are therefore small compared to the rigidity introduced by the tangled field throughout the star, and the $l = 1$ modes are unchanged to two significant figures. A simple analysis is given in Appendix B that further quantifies this effect. By contrast, the rigidity of the crust is essential an essential ingredient if the field is not significantly tangled, as considered in previous work (*e.g.*, van Hoven & Levin 2011; Colaiuda & Kokkotas 2011; Gabler et al. 2011, 2012; van Hoven & Levin 2012; Gabler et al. 2013a,b, 2014).

On the balance, stratification has a larger effect than does the crust. The combined effects of stratification and a crust is presented in Table 4, where the percentage change in frequencies compared with a constant density star of 13.1 km radius are given. For the $n = 0$ modes, the combined effects of stratification and a crust increase frequencies by up to 50%, because both effects add. For $n > 1$ the frequencies drop as a result of stratification, but are enhanced slightly by the crust giving a net change of up to 16%. Changes become more pronounced for increasing n , but less pronounced for increasing l .

We conclude that for star in which the tangled field accounts for much of the magnetic energy density ($b_t^2 \gtrsim 1$), that both density stratification and the crust rigidity have a relatively small effect on the frequencies of torsional normal modes. The constant-density model is an accurate first approximation at the 10% level for most overtones, and better than 50% for fundamental modes.

7 energetics

The only quantitative discussion to date of the energetics of QPO excitation has been given by Levin & van Hoven (2011). We use the results of their analysis to calculate the mode amplitude at the stellar surface in the global oscillation interpretation of QPOs, and the total energy in the low-frequency QPOs.

The natural candidate for the energy source that excites stellar modes is the flare itself. For giant flares, the energy cannot be released deep inside the star, as the impedance mismatch between the stellar interior and the magnetosphere is so great that the energy in Alfvén waves would take seconds or longer to reach the magnetosphere due to multiple reflections, in conflict with observed rise times of $\lesssim 10$ ms (Link 2014). This constraint favors an external origin for flares, as suggested by Lyutikov (2003, 2006), Komissarov et al. (2007), and Gill & Heyl (2010). Forcing of the magnetosphere through episodic release of *internal* magnetic energy could produce a magnetospheric explosion when an MHD instability is triggered.

Levin & van Hoven (2011) considered the excitation problem under the assumption that the magnetosphere undergoes a sudden change (over several relativistic Alfvén wave crossing times in the magnetosphere, $\sim 10^{-4}$ s) from one equilibrium configuration to another, exciting torsional oscillations in the star. Suppose the shear stress at the surface changes by $fB^2/4\pi$, where B is the characteristic field strength in the inner magnetosphere, and $f \leq 1$. The average displacement \bar{u}_i at the stellar surface, assuming excitation of *global* mode i with frequency ω_i , is of order (Levin & van Hoven 2011; eq. 11)

$$\frac{\bar{u}_i}{R} \sim \frac{1}{4\pi} \frac{fB^2 R}{M\omega_i^2} = \frac{3}{2\pi} \frac{fE_{\text{mag}}}{MR^2\omega_i^2} = 10^{-3} \left(\frac{fE_{\text{mag}}}{2 \times 10^{47} \text{ erg}} \right) \left(\frac{R}{10 \text{ km}} \right) \left(\frac{M}{1.4M_\odot} \right)^{-1} \left(\frac{\nu_i}{30 \text{ Hz}} \right)^{-2}, \quad (30)$$

where $E_{\text{mag}} \equiv (4\pi R^3/3)(B^2/8\pi) \sim 2 \times 10^{47} B_{15}^2$ erg is the characteristic magnetic energy available to be released; fE_{mag} is the total energy released, and should be comparable to the flare energy. The scaling as ω_i^{-2} follows from the Fourier transform of a step function.

The energy in a mode is of order (Levin & van Hoven 2011; eq. 12)

$$E_i \sim \frac{f^2 B^4 R^4}{32\pi^2 M \omega_i^2}. \quad (31)$$

Most of the energy is in low-frequency modes. We have found a fairly dense spectrum with a characteristic mode spacing of $\Delta\nu \simeq 10$ Hz. The sum of the total energy in all modes can be approximated with an integral

$$E \simeq \int_{\nu_0}^{\infty} d\nu \frac{E(\nu)}{\Delta\nu} \sim 10^{44} f^2 \left(\frac{B}{10^{15} \text{ G}} \right)^4 \left(\frac{R}{10 \text{ km}} \right)^4 \left(\frac{M}{1.4M_\odot} \right)^{-1} \left(\frac{\nu_0}{20 \text{ Hz}} \right)^{-1} \left(\frac{\Delta\nu}{10 \text{ Hz}} \right)^{-1} \text{ erg}, \quad (32)$$

where ν_0 is the lowest-frequency normal mode in the spectrum. We see that the conversion of magnetospheric energy to mechanical motion in the star is an inefficient process; about 0.1% of the flare energy goes into normal modes. The total energy in the modes in our model is well within the energy budget of a giant flare.

For a small flare, with $fE_{\text{mag}} = 10^{39}$ erg, the amplitude from eq. 30 is smaller by $\sim 10^8$ than if E_{mag} is liberated. These estimates hold not just for our model, but generally for any global-oscillation model of QPOs.

8 discussion and conclusions

We propose a new physical scenario for magnetar oscillations wherein the Alfvén continuum supported by the organized field is broken by nearly isotropic stresses arising from components of the field that form a complex tangle over scales much smaller than the stellar radius. In a simple model of constant density, an organized field of strength $\sim 10^{15}$ G, and a tangled field of comparable strength, a fundamental frequency appears near 20 Hz for $l = 1$ and $l = 2$, with a mode spacing of ~ 10 Hz (we use l from the solutions of the isotropic problem to label the modes of the anisotropic problem). The model is consistent with QPOs observed in SGRs 1806 and 1900 below about 160 Hz. Magnetic stresses dominate material stresses almost everywhere in the crust, so crust elasticity is unimportant when a strong, tangled field is present. We find that the combined effects of realistic stellar structure and crust stress give a modest change in the eigenfrequencies of $\sim 10\%$ for most modes (but up to 50% for low- l fundamentals) so our simple model with constant density is a good first approximation to studying tangled fields that elucidates the essential physics. The strength of the organized field, which should be approximately dipolar, is determined observationally. Once stellar mass and radius are fixed, the model has only one important free parameter: the ratio of the energy densities in tangled and organized fields.

Our results are insensitive to whether or not the protons are superconducting. The upper critical field for type II superconductivity is $\lesssim 10^{16}$ G, comparable to average fields we find to be consistent with the QPOs observed in SGRs 1806 and 1900; the magnetic stress is nearly the same if the protons are superconducting, though we have assumed for definiteness that they are normal. Also, if the protons are superconducting, the neutrons are only slightly entrained by the protons throughout most of the core, and the dynamical mass density is nearly equal to the proton mass density in this case as well.

While our constant-density model is mostly illustrative, it is nevertheless sufficiently accurate to study torsional oscillations semi-quantitatively within our approximations; the model is able to account for *every* QPO observed in SGRs 1806 and 1900 to within 3 Hz. No other published model has given such quantitative agreement, though we acknowledge that the success of the model is due in large part to the rather dense spectrum we predict with a frequency spacing of about 10 Hz. We find the data are best explained if there is approximate equipartition of the energy in the smooth and tangled fields. Such modes have high enough wavenumbers to probe the field structure over scales below $0.2R$, at which point the averaging procedure we introduced to treat the tangled field might become inappropriate.

Why have most of the predicted frequencies not been observed? One possibility is that the modes have been excited, but are not visible. Given that we do not understand how surface oscillations affect magnetospheric emission, it could be that some modes are not seen because they do not produce sufficiently large changes in the x-ray emissivity to be visible from our viewing angle. Another possibility is that the instability that drives the flare creates highly-preferential excitation of axial modes. We note that preferential excitation of low-frequency free oscillations occurs in the Earth (Rhie & Romanowicz 2004), the so-called “hum”. The question of how preferential excitation of stellar modes might occur is an interesting question.

While our focus has been on SGRs 1806 and 1900, which have dipole fields of $\sim 10^{15}$ G, QPOs have been reported for SGR J1550-5418 (Huppenkothen et al. 2014) in association with burst storms. SGR J1550-5418 has an inferred dipole field of 3.2×10^{14} G (Camilo et al. 2007). In this object, as in SGR 1900, the observed QPOs can be accounted for if most of the magnetic energy is in the tangled field, so that the average magnetic field is $\sim 10^{15}$ G.

A crucial ingredient in the interpretation of QPOs as stellar oscillations is to understand how crust movement can produce the large observed modulations of the x-ray emission by 10-20%. Timokhin et al. (2008) propose that twisting of the crust, associated with a stellar mode, modulates the charge density in the magnetosphere, creating variations in the optical depth for resonant Compton scattering of the hard x-rays that accompany the flare. In that model, the shear amplitude at the stellar surface must be as large as 1% of the stellar radius. D’Angelo & Watts (2012) accounted for geometrical effects of the beamed emission, and find that the amplitude of the QPO emission is increased by a factor of typically several over the estimate of Timokhin et al. (2008) for a given amplitude of the surface displacement. Based on the analysis of Levin & van Hoven (2011) of mode excitation by a sudden change in magnetospheric equilibrium, we find that the predicted, low-frequency QPO spectrum could contain up to $\sim 10^{44}$ erg in mechanical energy. This number is well within the energy budget of giant flares but the surface amplitude is only $\sim 10^{-3}R$ ($30 \text{ Hz}/\nu$)², smaller than required by Timokhin et al. (2008), especially for the QPOs near 160 Hz. This small amplitude could spell trouble for the global-oscillation interpretation of QPOs, unless a more efficient mechanism than that of Timokhin et al. (2008) can be identified. Explaining QPOs in small bursts ($\sim 10^{39}$ erg) appears particularly difficult with a global oscillation model. The mode amplitude scales as the flare energy (eq. 30), giving a surface amplitude that is $\sim 10^8$ times smaller than for a giant flare. The 626 Hz QPO reported in SGR 1806 also seems problematic to excite in a giant flare, with a surface amplitude of $\sim 10^{-6}R$ in the most optimistic case. These numbers show that energetics should be given serious consideration in QPO models, and that other excitation mechanisms than that of Levin & van Hoven (2011) should be considered.

The simple model presented in this paper can be improved by including a crust and introducing realistic stellar structure. We have shown that the effects typically ~ 10 for most modes for a star in which the magnetic energy density is dominated by that in the tangled field; the effects of stellar structure and the crust will become more important as the effective shear modulus from the tangled field is reduced, and we have not quantified these effects. Other modes than axial modes, such as polar modes, should be considered as well.

An explanation for why the observed frequencies are quasi-periodic is well beyond the scope of our model. Quasi-periodicity could arise from magnetospheric effects, dynamics in the star not included here, or both.

ACKNOWLEDGMENTS

We thank M. Gabler, D. Huppenkothen, Y. Levin, and A. Watts for very helpful discussions, and Y. Levin and A. Watts for comments on the manuscript. This work was supported by NSF Award AST-1211391 and NASA Award NNX12AF88G.

APPENDIX A: VARIABLE SEPARATION

Eqs. (25) and (26) can be separated and solved by transforming to an oblate spheroidal coordinate system (u, v) defined by

$$s = R \sqrt{\frac{(1 + b_t^2 u^2)(1 - v^2)}{1 + b_t^2}} \quad (\text{A1})$$

$$z = Ruv \quad (\text{A2})$$

Curves of constant u are ellipses, and curves of constant v are hyperbolae. For $u = 1$, the coordinate gives a sphere of radius R . In the limit $b_t^2 \rightarrow \infty$, spherical coordinates are recovered with $u = r/R$ and $v = \cos \theta$.

In these coordinates, eq. (25) becomes

$$(1 + b_t^2 u^2) \frac{\partial^2 u_\phi}{\partial u^2} + 2b_t^2 u \frac{\partial u_\phi}{\partial u} + \frac{b_t^2 u_\phi}{1 + b_t^2 u^2} + b_t^2 (1 - v^2) \frac{\partial^2 u_\phi}{\partial v^2} - 2b_t^2 v \frac{\partial u_\phi}{\partial v} - \frac{b_t^2 u_\phi}{1 - v^2} + \bar{\omega}^2 (b_t^2 u^2 + v^2) u_\phi = 0$$

where

$$\bar{\omega} \equiv \frac{R\omega}{c_t} \sqrt{\frac{b_t^2}{1 + b_t^2}}, \quad (\text{A3})$$

and $c_t^2 \equiv \langle B_t^2 \rangle / (4\pi\rho_d)$.

The boundary condition eq. (26) at $u = 1$ becomes

$$(1 + b_t^2) \frac{\partial u_\phi}{\partial u} - b_t^2 u_\phi = 0, \quad (\text{A4})$$

while at $z = 0$ we require

$$u_\phi = 0, \quad (\text{A5})$$

for odd parity modes or

$$(1 + b_t^2 u^2) v \frac{\partial u_\phi}{\partial u} + b_t^2 (1 - v^2) u \frac{\partial u_\phi}{\partial v} = 0, \quad (\text{A6})$$

for even parity modes.

We seek a separable solution of the form

$$u_\phi(u, v) = U(u)V(v). \quad (\text{A7})$$

Eq. (A3) becomes

$$(1 + b_t^2 u^2) \frac{d^2 U}{du^2} + 2b_t^2 u \frac{dU}{du} + \frac{b_t^2 U}{1 + b_t^2 u^2} - \kappa b_t^2 U + \bar{\omega}^2 b_t^2 u^2 U = 0 \quad (\text{A8})$$

$$b_t^2 (1 - v^2) \frac{d^2 V}{dv^2} - 2b_t^2 v \frac{dV}{dv} - \frac{b_t^2 V}{1 - v^2} + \kappa b_t^2 V + \bar{\omega}^2 v^2 V = 0, \quad (\text{A9})$$

where κ is the separation constant. The boundary condition eq. (A4) becomes

$$(1 + b_t^2) \frac{dU}{du} - b_t^2 U = 0, \quad (\text{A10})$$

at $u = 1$. The boundary conditions (A5) and (A6) are satisfied if we impose

$$U(0) = 0 \quad \text{and} \quad V(0) = 0, \quad (\text{A11})$$

for odd parity modes or

$$U'(0) = 0 \quad \text{and} \quad V'(0) = 0, \quad (\text{A12})$$

for even parity modes.

In the limit $b_t^2 \rightarrow \infty$, eq. (A8) reduces to the spherical Bessel equation with solution $U(u) = j(\bar{\omega}u)$, while (A9) reduces to an associated Legendre equation with solution $V(v) = \sqrt{1 - v^2} \partial P_l^0 / \partial v = -P_l^1(v)$ and $\kappa = l(l + 1)$, which recovers the solutions of the isotropic model of §4.

We solve eqs. (A8), (A9), (A10) numerically for the normal mode frequencies.

For arbitrary b_t^2 the modes are identified by the number of nodes; for the n^{th} mode the function $U(u)$ has n nodes on the domain $0 \leq u \leq 1$, while for the l^{th} mode the function $V(v)$ has $l - 1$ nodes on $-1 \leq v \leq 1$.

APPENDIX B: EFFECTS OF THE CRUST

The comparisons to observed QPOs in §5 suggest $b_t^2 \sim 1$, so that $\langle B_t^2 \rangle / 4\pi \sim B_o^2 / 4\pi \simeq 8 \times 10^{28} \text{ erg cm}^{-3}$. The shear modulus crust exceeds this value only in the densest regions of the crust. The rigidity of the crust will increase the normal-mode frequencies somewhat with respect to what we have found by neglecting the crust. Here we show that crust rigidity has small or negligible effects on our results.

To estimate the effect, we consider a two-component isotropic model with only a tangled field. The core liquid, which we

take to be homogeneous, has an effective shear modulus $\mu_{\text{core}} \equiv \langle B_t^2 \rangle / 4\pi$ and a shear-wave speed c_t . The crust, which we also take to be homogeneous, has shear modulus μ_{crust} and a shear-wave speed c_μ . The crust has an inner radius R_c and outer radius R .

In the core, the solution to the mode problem is $u_{\text{core}} = j_l(kr)$; the mode frequency is $\omega = c_t k$. The solution in the crust is $u_{\text{crust}} = a j_l(k'r) + b n_l(k'r)$, where n_l are spherical Neumann functions, a and b are constants, and $\omega = c_\mu k'$. The boundary conditions are continuity in value and traction at $r = R_c$, and vanishing traction at $r = R$:

$$u_{\text{core}}(R_c) = u_{\text{crust}}(R_c), \quad (\text{B1})$$

$$\mu_{\text{core}} \left[\frac{du_{\text{core}}}{dr} - \frac{u_{\text{core}}}{r} \right]_{r=R_c} = \mu_{\text{crust}} \left[\frac{du_{\text{crust}}}{dr} - \frac{u_{\text{crust}}}{r} \right]_{r=R_c}, \quad (\text{B2})$$

$$\mu_{\text{crust}} \left[\frac{du_{\text{crust}}}{dr} - \frac{u_{\text{crust}}}{r} \right]_{r=R} = 0. \quad (\text{B3})$$

The shear modulus in the crust, ignoring magnetic effects, is (Strohmayer et al. 1991)

$$\mu = \frac{0.1194}{1 + 0.595(173/\Gamma)^2} \frac{n_i (Ze)^2}{a}, \quad (\text{B4})$$

where n_i is the number density of ions of charge Ze , a is the Wigner-Seitz cell radius given by $n_i 4\pi a^3 / 3 = 1$, and $\Gamma \equiv (Ze)^2 / (akT)$ where k is Boltzmann's constant. Typically in the crust, $\Gamma \gg 173$ and the second term in the denominator is negligible. For the composition of the inner crust, we use the results of Douchin & Haensel (2001), conveniently expressed analytically by Haensel & Potekhin (2004). We solve for crust structure using the Newtonian equation for hydrostatic equilibrium, for a stellar radius of 10 km and a stellar mass of $1.4 M_\odot$. In the evaluation of the shear-wave speed in the crust, we include the effects of nuclear entrainment (Chamel 2005, 2012). Further details are given in Link (2014).

We find that μ_{crust} drops from $2 \times 10^{30} \text{ erg cm}^{-3}$ at the base of the crust to $8 \times 10^{28} \text{ erg cm}^{-3}$ over 370 m. Because we have assumed a homogeneous crust, we take the geometric mean of μ_{crust} over this range, which is $4 \times 10^{29} \text{ erg cm}^{-3}$, and set the crust thickness to 370 m. (The matter in the remainder of the crust contributes less to the rigidity than does the tangled field). The shear speed in the crust varies by a factor of about two in this region, with a geometric mean of $5 \times 10^{-3} c$. With these values, we solve the boundary conditions numerically for the corrected eigenfrequencies. Crust rigidity increases the mode frequency by $\lesssim 12\%$ for each fundamental of a given l , and $\lesssim 3\%$ for harmonics.

The treatment by Douchin & Haensel (2001) of the inner crust gives somewhat higher values of the shear modulus at the base of the crust than do other studies. The equation of state of Akmal et al. (1998), for example, gives a shear speed at the base of the crust that is about 0.6 the shear speed of Douchin & Haensel (2001), and a corresponding shear modulus that is smaller by a factor of about 2.8. Reducing the crust shear modulus by a factor of two, and repeating the above analysis, shows that crust rigidity increases the fundamental frequency for each l by less than 10%.

REFERENCES

- Akmal A., Pandharipande V., Ravenhall D., 1998, *Physical Review C*, 58, 1804
 Barat C., Chambon G., Hurley K., Niel M., Vedrenne G., Estulin I., Kurt V., Zenchenko V., 1979, *Astronomy and Astrophysics*, 79, L24
 Camilo F., Ransom S., Halpern J., Reynolds J., 2007, *The Astrophysical Journal Letters*, 666, L93
 Cerdá-Durán P., Stergioulas N., Font J. A., 2009, *Mon. Not. Roy. Astron. Soc.*, 397, 1607
 Cerdá-Durán P., Stergioulas N., Font J. A., 2009, *Monthly Notices of the Royal Astronomical Society*, 397, 1607
 Chamel N., 2005, *Nucl. Phys. A*, 747, 109
 Chamel N., 2012, *Phys. Rev. C*, 85, 035801
 Chamel N., Haensel P., 2006, *Phys. Rev. C*, 73, 045802
 Cline T., Desai U., Pizzichini G., Teegarden B., Evans W., Klebesadel R., Laros J., Hurley K., Niel M., Vedrenne G., 1980, *The Astrophysical Journal*, 237, L1
 Colaiuda A., Beyer H., Kokkotas K., 2009, *Monthly Notices of the Royal Astronomical Society*, 396, 1441
 Colaiuda A., Kokkotas K., 2012, *Monthly Notices of the Royal Astronomical Society*, 423, 811
 Colaiuda A., Kokkotas K. D., 2011, *Mon. Not. Roy. Astron. Soc.*, 414, 3014
 D'Angelo C., Watts A., 2012, *The Astrophysical Journal Letters*, 751, L41
 Douchin F., Haensel P., 2001, *Astron. Astrophys.*, 380, 151
 Duncan R. C., 1998, *Astrophysics J.*, 489, L45
 El-Mezeini A. M., Ibrahim A. I., 2010, *Astrophys. J. Lett.*, 721, L121
 Fenimore E. E., Klebesadel R. W., Laros J. G., 1996, *Astrophys. J.*, 460, 964

- Feroci M., Frontera F., Costa E., Amati L., Tavani M., Rapisarda M., Orlandini M., 1999, *The Astrophysical Journal Letters*, 515, L9
- Gabler M., Cerdá-Durán P., Font J. A., Müller E., Stergioulas N., 2013a, *Monthly Notices of the Royal Astronomical Society*, 430, 1811
- Gabler M., Cerdá-Durán P., Stergioulas N., Font J. A., Müller E., 2012, *Monthly Notices of the Royal Astronomical Society*, 421, 2054
- Gabler M., Cerdá-Durán P., Stergioulas N., Font J. A., Müller E., 2013b, *Physical review letters*, 111, 211102
- Gabler M., Cerdá-Durán P., Stergioulas N., Font J. A., Müller E., 2014, *Monthly Notices of the Royal Astronomical Society*, 443, 1416
- Gabler M., Cerdá-Durán P., Font J. A., Müller E., Stergioulas N., 2011, *Mon. Not. Roy. Astron. Soc.*, 410, L37
- Gill R., Heyl J. S., 2010, *Monthly Notices of the Royal Astronomical Society*, 407, 1926
- Glampedakis K., Samuelsson L., Andersson N., 2006, *Mon. Not. Roy. Astron. Soc.*, 371, L74
- Goedbleed J. P. H., Poedts S., 2004, *Principles of Magnetohydrodynamics*. Cambridge Univ. Press, Cambridge
- Haensel P., Potekhin A. Y., 2004, *Astron. Astrophys.*, 428, 191
- Hambaryan V., Neuhauser R., Kokkotas K. D., 2011, *Astron. Astrophys.*, 528, 45
- Huppenkothen D., D'Angelo C., Watts A. L., Heil L., van der Klis M., van der Horst A. J., Kouveliotou C., Baring M. G., Göğüş E., Granot J., et al., 2014, *The Astrophysical Journal*, 787, 128
- Huppenkothen D., Heil L., Watts A., Göğüş E., 2014, *The Astrophysical Journal*, 795, 114
- Huppenkothen D., Watts A. L., Uttley P., van der Horst A. J., van der Klis M., Kouveliotou C., Göğüş E., Granot J., Vaughan S., Finger M. H., 2013, *The Astrophysical Journal*, 768, 87
- Hurley K., Cline T., Mazets E., Barthelmy S., Butterworth P., Marshall F., Palmer D., Aptekar R., Golenetskii S., Il'Inskii V., et al., 1999, *Nature*, 397, 41
- Israel G., Belloni T., Stella L., Rephaeli Y., Gruber D., Casella P., Dall'Osso S., Rea N., Persic M., Rothschild R., 2005, *The Astrophysical Journal Letters*, 628, L53
- Komissarov S., Barkov M., Lyutikov M., 2007, *Monthly Notices of the Royal Astronomical Society*, 374, 415
- Lee U., 2007, *Mon. Not. Roy. Astron. Soc.*, 374, 1015
- Levin Y., 2006, *Mon. Not. Roy. Astron. Soc.*, 368, L35
- Levin Y., 2007, *Mon. Not. Roy. Astron. Soc.*, 377, 159
- Levin Y., van Hoven M., 2011, *Monthly Notices of the Royal Astronomical Society*, 418, 659
- Link B., 2014, *Monthly Notices of the Royal Astronomical Society*, 441, 2676
- Lyutikov M., 2003, *Mon. Not. Roy. Astron. Soc.*, 346, 540
- Lyutikov M., 2006, *Monthly Notices of the Royal Astronomical Society*, 367, 1594
- Mazets E., Golenetskii S., Il'Inskii V., Aptekar R., Guryan Y. A., 1979, *Nature*, 282, 587
- Mereghetti S., Esposito P., Tiengo A., Zane S., Turolla R., Stella L., Israel G., Götz D., Feroci M., 2006, *The Astrophysical Journal*, 653, 1423
- Nakagawa Y. E., Mihara T., Yoshida A., Yamaoka K., Sugita S., Murakami T., Yonetoku D., Suzuki M., Nakajima M., Tashiro M., et al., 2008, *PASJ*, 61, S387
- Passamonti A., Lander S., 2013, *Monthly Notices of the Royal Astronomical Society*, 429, 767
- Passamonti A., Lander S. K., 2014, *MNRAS*, 438, 156
- Piro A. L., 2005, *Astrophys. J.*, 634, L153
- Potekhin A., Fantina A., Chamel N., Pearson J., Goriely S., 2013, *Astronomy & astrophysics*, 560, A48
- Rhie J., Romanowicz B., 2004, *Nature*, 431, 552
- Samuelsson L., Andersson N., 2007, *Mon. Not. Roy. Astron. Soc.*, 374, 256
- Sotani H., Colaiuda A., Kokkotas K. D., 2007, *Mon. Not. Roy. Astron. Soc.*, 385, 2162
- Sotani H., Kokkotas K. D., Stergioulas N., 2007, *Mon. Not. Roy. Astron. Soc.*, 375, 261
- Sotani H., Kokkotas K. D., Stergioulas N., 2008, *Mon. Not. Roy. Astron. Soc.*, 385, L5
- Steiner A. W., Watts A. L., 2009, *Phys. Rev. Lett.*, 103, 181101
- Strohmayer T. E., van Horn H. M., Ogata S., Iyemori H., Ichimaru S., 1991, *Astrophys. J.*, 375, 679
- Strohmayer T. E., Watts A. L., 2005, *Astrophys. J.*, 632, L111
- Strohmayer T. E., Watts A. L., 2006, *The Astrophysical Journal*, 653, 593
- Tiengo A., Esposito P., Mereghetti S., Israel G., Stella L., Turolla R., Zane S., Rea N., Götz D., Feroci M., 2009, *Mon. Not. Roy. Astron. Soc.*, 399, L74
- Timokhin A., Eichler D., Lyubarsky Y., 2008, *The Astrophysical Journal*, 680, 1398
- van Hoven M., Levin Y., 2011, *Mon. Not. Roy. Astron. Soc.*, 420, 1036
- van Hoven M., Levin Y., 2012, *Monthly Notices of the Royal Astronomical Society*, 420, 3035
- Watts A. L., Reddy S., 2007, *Mon. Not. Roy. Astron. Soc.*, 379, 63
- Watts A. L., Strohmayer T. E., 2006, *Astrophys. J.*, 637, L117